ISSN 1063-7834, Physics of the Solid State, 2019, Vol. 61, No. 12, pp. 2493–2502. © Pleiades Publishing, Ltd., 2019.
Russian Text © The Author(s), 2019, published in Fizika Tverdogo Tela, 2019, Vol. 61, No. 12, pp. 2462–2470.

METALS

Metastable Dispersed States Arising upon Three-Component Alloy Decomposition

I. K. Razumov[a, *] and Yu. N. Gornostyrev[a, b]

[a] *Mikheev Institute of Metal Physics, Ural Branch, Russian Academy of Sciences, Yekaterinburg, 620219 Russia*
[b] *Ural Federal University, Yekaterinburg, 620075 Russia*
**e-mail: rik@imp.uran.ru*

Received May 6, 2019; revised July 16, 2019; accepted July 16, 2019

Abstract—In this paper, we consider the conditions for inhibiting the growth of precipitates from a metastable supersaturated solid solution and at the evaporation-condensation stage during spinodal decomposition of a three-component alloy. The formation of a "locking" shell around precipitates was shown to be an effective mechanism for inhibiting decomposition, provided that the solubility or diffusion coefficients of the alloy components are reduced in the shell. The thermodynamic and kinetic conditions for the appearance of such shells are formulated. The features of decomposition inhibition mechanisms in specific alloys are discussed.

Keywords: spinodal decomposition, three-component alloy, dispersed states
DOI: 10.1134/S1063783419120436

1. INTRODUCTION

Considerable attention has recently been given to materials whose unique properties are achieved due to the formation of a structural state containing nanoscale precipitates. Known examples are aging martensitic steels [1, 2] and alloys based on aluminum [3], titanium [4], and transition metals with a composite structure [5]. A promising way to control the structural state is to use alloying elements that increase the stability of precipitates [6–9]. However, physical mechanisms ensuring the stability of dispersed states are not well understood. As the main factors, existing concepts distinguish elastic stresses [10, 11], the composition dependence of precipitates on their size, segregation of impurities at the interphase boundaries [12, 13], and the appearance of kinetically determined shells around precipitates [14].

The effect of the alloying element on the decomposition kinetics was investigated in a number of studies using the example of a three-component alloy. It was shown that, even when choosing the average concentration of the third component in the solubility region, the interphase boundary can be enriched by it due to the formation of a special state under conditions of local equilibrium [15, 16]. However, studies of this effect using the example of an alloy Fe–Cu–Ni (Mn, Al) showed that the boundary enrichment of Cu precipitates with Ni (Mn, Al) impurities has little effect on the growth kinetics of precipitates [16–18].

In the case of violation of the coherence of the lattice at the interface, it becomes similar to the grain boundary, and favorable conditions are created for the segregation of impurity atoms on it. In this case, anomalous disperse states with the equilibrium size of precipitates increasing with decreasing average impurity concentration can be formed [12]. Stabilization of Mg_2Sn precipitates due to Zn segregation at the interphase boundary was studied in detail and their equilibrium size was determined [13].

Both thermodynamic and kinetic factors play an important role in the formation of a dispersed structure. For example, the difference in the diffusion mobility of Zr and Sc in the Al–Sc–Zr alloy leads to the formation of a kinetically determined shell around $Al_3Sc_xZr_{1-x}$ precipitates, which blocks the coarsening of the microstructure [14]. Another situation was considered in [19], where the decomposition of a binary alloy with stationary particles of the third phase introduced into the initial state was simulated, the presence of which inhibited the decomposition. The formation of precipitates with a mixed composition was considered in [20], and the decomposition was shown to slow down if one of the impurities has a low diffusion coefficient.

In this paper, we consider the decomposition in a three-component alloy, with particular attention to mechanisms of growth restrictions of primary precipitates coherent with the matrix. The obtained results allow formulating the conditions under which a shell around the precipitates is formed and stabilization of the dispersed states of the alloy is achieved.

2. MODEL FORMULATION

In the mean field approximation, the functional of the free Ginzburg–Landau energy [10] for a three-component A–B–M alloy has the following form:

$$F = \int \{f(c_A, c_B) + E_{\text{surf}}\} d\mathbf{r}, \quad (1)$$

where $f(c_A, c_B)$ is the free energy density depending on the local concentrations $c_A(\mathbf{r})$ and $c_B(\mathbf{r})$, E_{surf} is the contribution to the surface energy due to concentration gradients; component concentrations are related by the condition: $c_A + c_B + c_M = 1$. The free energy density contains contributions related to the internal energy and configurational entropy [21]:

$$f(c_A, c_B) = g(c_A, c_B) + kT\sum_{\alpha} c_\alpha \ln c_\alpha. \quad (2)$$

The internal energy density has the following form:

$$g(c_F, c_B) = \sum_{\alpha} E_\alpha c_\alpha = g_0 + \varepsilon_A c_A + \varepsilon_B c_B + \nu_{AM} c_A^2 + \nu_{BM} c_B^2 + \nu c_A c_B, \quad (3)$$

where $g_0 = \text{const}$, ε_α is the energy of dissolution of the component α in the matrix, $\nu_{\alpha\beta}$ is the mixing energy of the components α and β; $\nu = \nu_{AM} + \nu_{BM} - \nu_{AB}$. Under the condition of $\nu_{\alpha M} < 0$, the possibility of decomposition with the precipitation of components $\alpha = \{A, B\}$ is provided while the energy ν characterizes the tendency of A and B atoms to form precipitates with a mixed composition ($\nu < 0$) or, conversely, to decompose ($\nu > 0$). The sequential derivation of expression (3) from the configurational Hamiltonian of a three-component alloy implies neglecting correlations in the atom arrangement and a smooth change in concentrations at distances of the order of the lattice parameter [22].

In the general case, ε_α differ in various phases, which can be taken into account by the concentration dependence of $\varepsilon_\alpha(c_A, c_B)$. We omit the linear contributions to (3), which do not affect the thermodynamics of the transformations, and move on to the effective mixing energies including the concentration dependence of quantities ε_α, $\nu_{\alpha M}$, and ν_{AB}:

$$g(c_A, c_B) = \tilde{\nu}_{AM}(c_A, c_B)c_A^2 + \tilde{\nu}_{BM}(c_A, c_B)c_B^2 + \tilde{\nu} c_A c_B(c_A, c_B). \quad (4)$$

We write down E_{surf} energy in the following form [23]:

$$E_{\text{surf}} = \frac{R^2}{2}(\sigma_A(\nabla c_A)^2 + \sigma_B(\nabla c_B)^2 + \sigma_{AB}(\nabla c_A \nabla c_B)). \quad (5)$$

Here, R is a parameter characterizing the width of the interphase boundary; σ_α are the energy coefficients determining the surface energy of the precipitates of types A and B; and σ_{AB} is the change in surface energy at contact of precipitates of different types. If σ_{AB} is greater the critical value, the E_{surf} energy becomes negative, and the realization of a phase transition of complete wetting should be expected [24]. In the general case, the energies σ_α can depend on the local concentrations of the alloy components, $\sigma_\alpha = \sigma_\alpha^{(0)} + \sigma_{\alpha\beta}c_\beta + \cdot$, leading to contributions to a functional of the form $c_\beta(\nabla c_\alpha)^2$ responsible for impurity segregation at the interphase boundaries [12]. In this study, we restrict ourselves to the analysis of the $E_{\text{surf}} > 0$ case and will not take into account the gradient contributions of more high order in equation (5).

To describe the evolution of concentrations, we use continuity equations [21]:

$$\frac{\partial c_{A(B)}}{\partial t} = -\nabla J_{A(B)}. \quad (6)$$

The atom fluxes $J_{A(B)}$ are determined by a linear combination of the gradients of the chemical potentials of all components, $J_i = -c_i M_{ij}\nabla(\delta F/\delta c_j)$. In this case, Onsager relations $M_{ij} = M_{ji}$ are fulfilled for the off-diagonal components of the mobility matrix [21]. Since diagonal elements usually make the determining contribution, we assume that $M_{ij} = M_{ji} = 0$ at $i \neq j$, so that

$$J_{A(B)} = -\frac{D_{A(B)}(c_A, c_B)c_{A(B)}c_M}{kT}\nabla\left(\frac{\delta F}{\delta c_{A(B)}}\right). \quad (7)$$

The diffusion coefficients of the components differ in various phases while their rapid change occurs at the interface, which can be accounted phenomenologically as follows:

$$D_\alpha = D_\alpha^{(M)} + (D_\alpha^{(\beta)} - D_\alpha^{(M)})\left[1 + \exp\left(\frac{c_\beta^{\text{cr}} - c_\beta}{\lambda}\right)\right], \quad (8)$$

where $D_\alpha^{(M)}$ and $C_\alpha^{(\beta)}$ are the diffusion coefficients of atoms of type $\alpha = \{A, B\}$ in the matrix and precipitates of type β, respectively, c_β^{cr} is the threshold concentration corresponding to the appearance of phase β, and $\lambda \sim 0.01$ is the small parameter. For simplicity, the self-diffusion coefficients are assumed to be equal to the diffusion coefficients in the matrix, i.e., $D_\alpha^{(\alpha)} \approx D_\alpha^{(M)}$.

An analysis of expression (7) allows drawing general conclusions about the conditions for precipitate stabilization during alloy decomposition. The thermodynamically equilibrium dispersed state arises when the chemical potentials of the components are independent of coordinates ($\delta F/\delta c_\alpha = \text{const}$). Such a state can be realized due to the elastic interaction of precipitates [10, 11] or as a result of impurity segregation at interphase boundaries [12, 13]. The kinetic mechanism of stabilization of precipitates is realized if the factor in front of the gradient in equation (7) becomes small, which is achieved if the precipitate is surrounded by a shell, in which the diffusion coefficients ($D_{A(B)} \approx 0$) or the equilibrium concentration ($c_{A(B)} \approx 0$)

of alloy components are small. Fulfillment of these conditions should be expected when the shell forming around the precipitate is a new phase.

When solving equations (6) numerically, we use a two-layer explicit finite-difference scheme for a square 2D region, with dimensionless time $\tau = tD_A^{(M)}/L^2$ and coordinates x/L (L is the size of the calculation domain). When analyzing a solution, it is convenient to use an integral degree of the decomposition for component A:

$$S_{\text{dec}} = \frac{1}{2c_A^0(1-c_A^0)L^d}\int\left|c_A(\mathbf{r}) - c_A^0\right|d\mathbf{r}, \qquad (9)$$

where d is the dimension of the problem, c_A^0 is the sample-averaged concentration of component A, and $0 \le S_{\text{dec}} \le 1$. To characterize the dispersion degree of precipitates, we use the following value:

$$S_{\text{disp}} = \frac{R^2}{L^d}\int\sqrt{(\nabla c_A(\mathbf{r}))^2}d\mathbf{r}. \qquad (10)$$

3. IMPURITY SHELLS AROUND PRECIPITATES IN BIPHASIC ALLOYS

3.1. Kinetically Determined Shell

Let us first consider the growth of a single precipitate from the metastable supersaturated solid solution (the figurative point on the phase diagram is between the binodal and spinodal [21]) in the simplest case, when $\tilde{\nu}_{AM} < 0$, $\tilde{\nu}_{BM} = \tilde{\nu} = 0$. Let the average impurity concentration c_B^0 be higher than the equilibrium solubility limit of component A in the matrix $c_{A\_\text{eqv}}^{(M)}$. Then, component B is displaced from the growing precipitate A to the matrix. In this case, if the diffusion rate of component B is small in the matrix ($D_B^{(M)} \ll D_A$) and is quite large in the precipitate volume ($D_B^{(A)} \sim D_A$), a shell with a high concentration of component B appears around the precipitate at the intermediate stage of transformation. Assuming in this section an axial symmetry of the problem, we use cylindrical coordinates when solving of equation (6). The calculated concentration profiles are presented in Fig. 1a. Germination of precipitate A through the formed shell is impossible since the decomposition conditions are locally violated at a high concentration of component B (the figurative point in the phase diagram of the alloy is shifted to the solubility region of component A). Therefore, further evolution requires either a displacement or dissolution of the shell, which is limited by a low coefficient $D_B^{(M)}$. As a result, the decomposition rate decreases significantly (compare curves *1* and *2* plotted in the absence and presence of a shell in Fig. 1b).

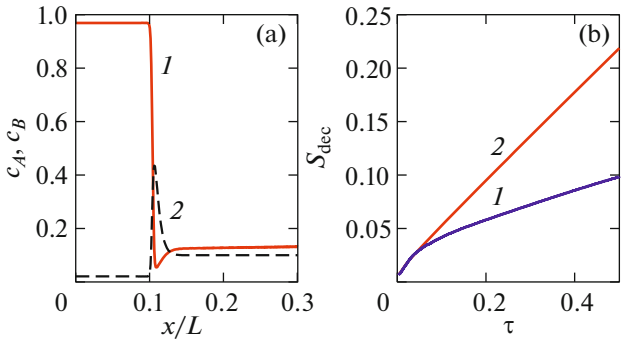

Fig. 1. (a) Concentration distribution of components (*1*) A and (*2*) B at the time instant of $\tau = 2.65$ and $D_B^{(M)}/D_A = 10^{-4}$, $D_B^{(A)}/D_A = 3$; (b) evolution of the decomposition extent at $D_B^{(M)}/D_A = 10^{-4}$, $D_B^{(A)}/D_A = 3$ (*1*); $D_B/D_A = 10^{-4}$ (*2*). $\tilde{\nu}_{AM}/kT = -4$, $\tilde{\nu}_{BM} = \tilde{\nu} = 0$, $c_A^0 = 0.15$, $c_B^0 = 0.10$, $\sigma_{A(B)}(R/L)^2/kT = 10^{-5}$, $\sigma_{AB} = 0$; x is the distance to the sample center.

3.2. Enrichment of the Interphase Boundary with an Impurity at the Interaction of Components A and B

Let us consider the more general case $\tilde{\nu}_{AM} < 0$, $\tilde{\nu} < 0$, $\tilde{\nu}_{BM} = 0$, for which the internal energy $g = \tilde{\nu}_{AM}c_A^2 + \tilde{\nu}c_Ac_B$ decreases due to the clustering of both atoms of type A and atoms of different types A and B. If $\tilde{\nu}/\tilde{\nu}_{AM} > 1$, the ratio of the equilibrium concentrations of component B in the matrix and the precipitate volume is $c_{B\_\text{eqv}}^{(A)}/c_{B\_\text{eqv}}^{(M)} > 1$. In this case, the concentration of c_B at the interface exhibits an unusual behavior, many times exceeding the equilibrium values of $c_{B\_\text{eqv}}^{(A)}$, $c_{B\_\text{eqv}}^{(M)}$. As a result, a shell enriched with component B is formed at the interphase boundary (Fig. 2a). At lowering the temperature or increasing the concentration c_A^0, the figurative point moves to the region of the phase diagram below the spinodal dome, and the spinodal decomposition occurs in the alloy, during which precipitates with an interphase boundary enriched with component B are also formed (Fig. 2b).

The formation of such a shell finds a simple explanation. From the condition that the chemical potential of component B at the interface is constant upon reaching local equilibrium, under simplifying assumptions $c_{A\_\text{eqv}}(x) \gg c_{A\_\text{eqv}}^{(M)}$ and $c_{B\_\text{eqv}}^{(M)} \ll 1$, it is easy to obtain an expression relating the equilibrium concentrations of impurities at the interface:

$$c_{B\_\text{eqv}}(C_{A\_\text{eqv}}) = \frac{(1-c_{A\_\text{eqv}}(x))c_{B\_\text{eqv}}^{(M)}}{c_{B\_\text{eqv}}^{(M)} + \exp\left[\dfrac{\tilde{\nu}c_{A\_\text{eqv}}(x)}{kT}\right]}. \qquad (11)$$

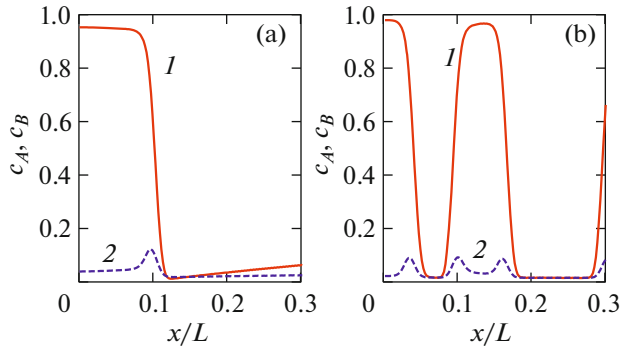

Fig. 2. Distributions of components (1) A and (2) B in the case of (a) the growth of the precipitate from a metastable supersaturated solution at $c_A^0 = 0.10$, $\tau = 0.08$, and (b) at spinodal decomposition at $c_A^0 = 0.25$, $\tau = 0.32$. $c_B^0 = 0.03$, $D_B/D_A = 1$, $\tilde{\nu}_{AM}/kT = -5$, $\tilde{\nu}/kT = -6$, $\tilde{\nu}_{BM} = 0$, $\sigma_{A(B)}(R/L)^2/kT = 4 \times 10^{-4}$, $\sigma_{AB} = 0$; x is the distance to the precipitate center.

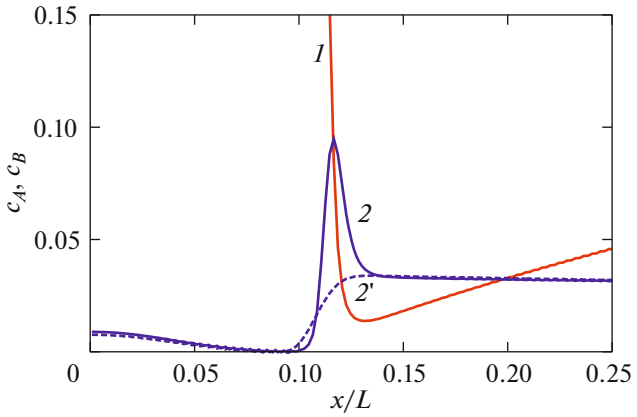

Fig. 3. Distributions of components (*1*) A and (*2*, *2'*) B at the growth of the precipitate from a metastable supersaturated solution at $\tilde{\nu} = 0$, $\sigma_{AB}(R/L)^2/kT =$ (*2*) 7×10^{-4} and (*2'*) 0; $\tau = 0.10$. The remaining parameters are similar as those in Fig. 2a.

As can be seen from this, the dependence $c_{B\_eqv}(c_{A\_eqv})$ is nonmonotonic, so that the concentration c_{B_eqv} can be significantly higher than that in the volume of phases at an intermediate concentration value of c_{A_eqv} (i.e., in the region of the interphase boundary).

It is easy to show that this shell leads to decomposition inhibition if the diffusion coefficient of component A decreases in the shell, blocking the matter supply to the growing precipitate. However, it is difficult to expect the realization of this condition if the formed shell is not a new phase.

Note that, qualitatively, a similar shell arises even in the case of $\tilde{\nu} = 0$, but in the presence of a gradient contribution to the wetting energy ($\sigma_{AB} > 0$). As seen in Fig. 3, in the case of $\sigma_{AB} > 0$, the interface is enriched with component B (curve *2*) while the concentration of component B monotonically changes at transition from one phase to another (curve *2'*) at $\sigma_{AB} = 0$.

Thus, each of the energy factors characterizing the tendency to the decomposition ($\tilde{\nu} < 0$) or "wetting" of the interphase boundary ($\sigma_{AB} > 0$) can lead to the enrichment of the interphase boundary with component B. The shell formation studied earlier in the numerical simulation [16] for the Fe–Cu–Ni(Mn) alloy was apparently due to the combined effect of these factors.

4. A PURE COMPONENT SHELL. PRECIPITATE PINNING

Let us consider an alloy with thermodynamic stimuli for the formation in the matrix of precipitates of both types A and B. Note that these stimuli vanish at a sufficiently large (modulo) value of $\tilde{\nu} < 0$, since the tendency to decompose into components A and B in this case is replaced by the formation of a phase with a mixed composition A–B (see discussion in [20]). On the contrary, in the case of $\tilde{\nu} > 0$, stimuli of decomposition in components A and B are enhanced. The following results relate to a characteristic scenario when $\tilde{\nu} = 0$, so that the internal energy of the alloy has the following form $g = \tilde{\nu}_{AM}c_A^2 + \tilde{\nu}_{BM}c_B^2$, $\tilde{\nu}_{\alpha M} < 0$. First, we consider the growth of the single precipitate A from a metastable supersaturated solid solution, assuming that the figurative point of the alloy is between the binodal and the spinodal (for both components). In the process of increasing precipitate A, component B is forced out of its volume into the adjacent region of the matrix where at some moment selection of type B. Let $c_{A\_eqv}^{(M)}$, $c_{A\_eqv}^{(B)}$ be equilibrium the concentration of component A in the matrix and in the volume of precipitates B. If prior to the formation of precipitate B, the growth rate of precipitate A according to (7) is determined by $c_{A\_eqv}^{(M)}$, then, after the occurrence of precipitate of B, the rate of substance supply to precipitate A is determined by the concentration $c_{A\_eqv}^{(B)}$. In this case, if the mixing energy $\tilde{\nu}_{BM}$ in absolute value significantly exceeds $\tilde{\nu}_{AM}$, the $c_{A\_eqv}^{(B)} \ll c_{A\_eqv}^{(M)}$ relation between equilibrium concentrations, which prevents further increase in precipitate A, is established.

Figures 4a and 4b present the various stages of the process under consideration: the increase in the initial precipitate A and the formation of precipitate B. Figure 4d shows the evolution of the decomposition extent for component A. As can be seen in the figure, the precipitate A monotonically increases in the absence of precipitate B. However, the growth almost stops after the formation of precipitate B.

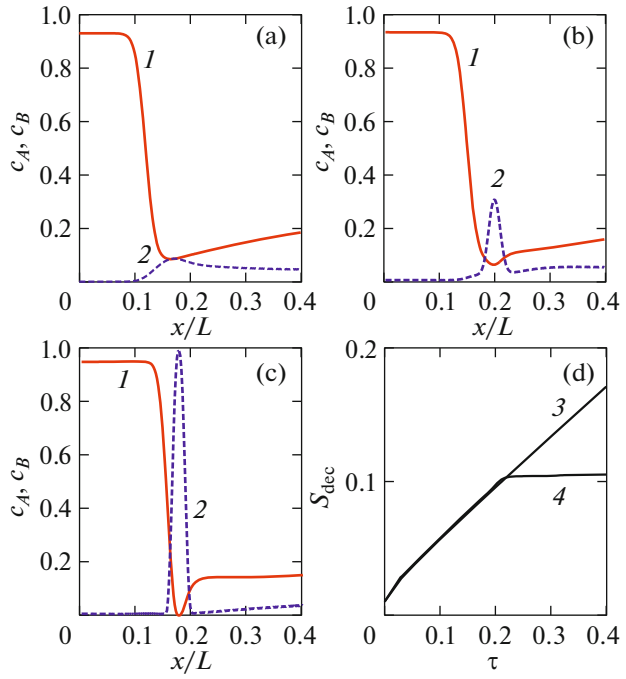

Fig. 4. Kinetics of decomposition with the formation of precipitates (*1*) *A* and (*2*) *B* at times of $\tau =$ (a) 0.11, (b) 0.20, (c) 0.25, and the evolution of the decomposition degree of component (d) *A* at (*3*) $\tilde{\nu}_{BM} = 0$, and (*4*) $\tilde{\nu}_{BM}/kT = -7$. $D_B/D_A = 1$, $\tilde{\nu}_{AM}/kT = -3$, $\tilde{\nu}_{BM}/kT = -7$, $\tilde{\nu} = 0$, $\sigma_{AB} = 0$, $\sigma_{A(B)}(R/L)^2/kT = 4 \times 10^{-4}$ eV, $c_A^0 = 0.2$, $c_B^0 = 0.05$.

At an increase in average concentrations c_A^0 and c_B^0 or upon lowering the temperature, the spinodal decomposition (SD) of one or both components occurs in the alloy. In this case, to form the structure of precipitates *A* surrounded by the shell of *B*, the situation when c_A^0 lies in the spinodal region of the diagram while c_B^0 lies in the metastable region of the diagram is favorable, then the decomposition of component *B* occurs only in the vicinity of precipitates *A* after displacing component *B* from them and does not develop in the matrix volume.

The above considered problem with the cylindrical symmetry allows analyzing the conditions of the shell formation, but does not take into account the possibility of the development of the decomposition along the interface. Therefore, from here we consider the solution of equations (6) inn a 2D region in Cartesian coordinates by introducing small randomly distributed Gaussian compositional fluctuations into the initial state and using periodic boundary conditions.

In the absence of diffusion of component *B* ($D_B = 0$), the spinodal decomposition of component *A* occurs [22]. The decomposition kinetics in the case of slow diffusion of component *B* ($D_B^{(M)}/D_A \ll 1$) is presented in Fig. 5. Precipitates *A* are highlighted in gray, precipitates *B* are highlighted in black, and the matrix phase is highlighted in white. As can be seen in the figure, chains of small precipitates *B* are formed around precipitates *A*. In this case, the germination of precipitates *A* between neighboring precipitates *B* is difficult because it is accompanied by a significant increase in surface energy. This results in a situation qualitatively similar to the pinning of grain boundaries with fine precipitates. Note that, at a high diffusion rate of component *B* in the matrix ($D_B^{(M)}/D_A > 1$), on the contrary, the decomposition of component *B* first occurs, and then precipitates *A* easily grow between randomly distributed precipitates *B* [19].

Figure 6 shows the change in the size of the maximal precipitate and the dispersion extent of precipitates at various ratios of diffusion coefficients of components *A* and *B*. As can be seen in the figure, the most effective stabilization of the dispersed state is achieved when atoms of type *B* quickly diffuse from the volume of precipitates *A*, but lose their mobility in the matrix ($D_B^{(A)}/D_A \sim 1$, $D_B^{(M)}/D_A \ll 1$).

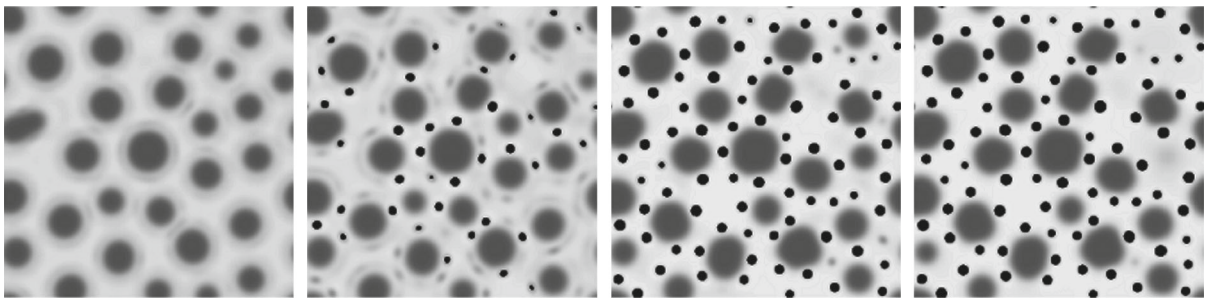

Fig. 5. Kinetics of spinodal decomposition at $c_A^0 = 0.30$, $c_B^0 = 0.08$, $\tilde{\nu}_{AM}/kT = -3$, $\tilde{\nu}_{BM}/kT = -7$, $\tilde{\nu} = 0$, $\sigma_{A(B)}(R/L)^2/kT = 4 \times 10^{-4}$, $\sigma_{AB} = 0$, $D_B^{(M)}/D_A = 10^{-2}$, $D_B^{(A)}/D_A = 1$, and $D_A =$ const.

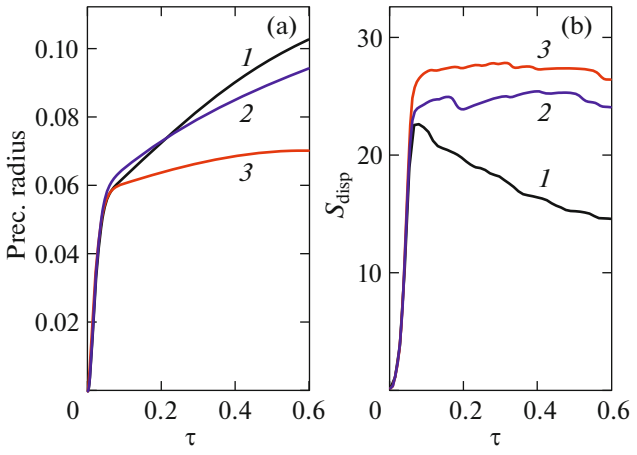

Fig. 6. Evolution of (a) the maximal size of the precipitate and (b) the dispersion extent of precipitates at (*1*) $D_B = 0$, (*2*) $D_B^{(M)} = 10^{-2}$, $D_B^{(A)}/D_A = 10^{-2}$, (*3*) $D_B^{(M)}/D_A = 10^{-2}$, and $D_B^{(A)}/D_A = 1$. The remaining parameters are similar as those in Fig. 5.

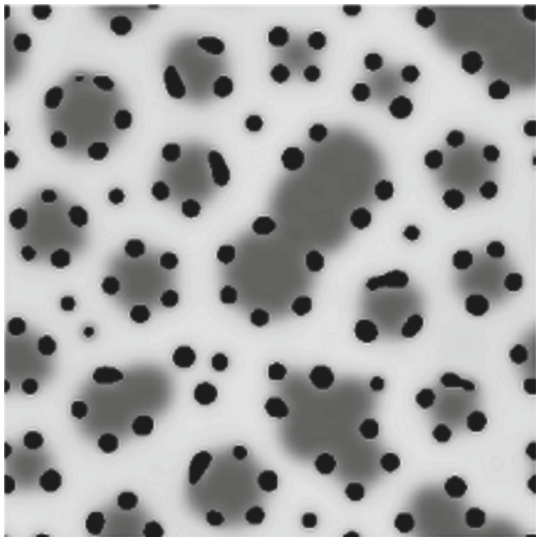

Fig. 7. Distribution of precipitates by the time of $\tau = 0.60$ at $c_B^0 = 0.12$, $\tilde{\nu} = -3$, and $\sigma_{A(B)}(R/L)^2/kT = 2 \times 10^{-4}$. The remaining parameters are similar as those in Fig. 5.

Taking into account the parameters $\tilde{\nu}$ and σ_{AB} responsible for the wetting processes does not change the qualitatively observed pattern (Fig. 7). Precipitates of component *B* are located in the surface layer of precipitates of *A*. However, the condition $\tilde{\nu}_{BM} < \tilde{\nu}_{AM}$ necessary for decomposition inhibition in the case under discussion leads to the formation of a discontinuous rather than continuous shell. In this case, if σ_{AB} exceeds the critical value, the surface energy (5) becomes negative during the phase contact, and the model under consideration loses its applicability.

Thus, the combined effect of thermodynamic and kinetic factors ensuring the formation of particles of a new phase at the interface of primary precipitates can serve as the effective decomposition-inhibition mechanism, even if a continuous shell around the precipitate is not formed.

5. SHELL FORMED BY PHASES WITH AN INTERMEDIATE COMPOSITION

In the general case, the mixing energies $\tilde{\nu}_{\alpha\beta}$ in formula (4) can be functions of concentrations, which may lead to a large variety of microstructures. In this case, a typical situation both in a binary alloy and in a three-component alloy is the formation of the phase with an intermediate composition. Let us consider as an example the case when decomposition of both components is possible in the alloy ($\tilde{\nu}_{AM} < 0$, $\tilde{\mu}_{BM} < 0$) while the energy $\tilde{\mu}_{BM}$ depends on the concentrations as follows:

$$\tilde{\nu}_{BM} = \tilde{\nu}_{BM}^0 + \tilde{\nu}_{BM}^{(A)} c_A + \tilde{\nu}_{BM}^{(M)} c_M + \tilde{\nu}_{BM}^{(AM)} c_A c_M + \ldots. \quad (12)$$

For the formation of a shell around precipitates *A*, it is necessary to ensure the cooperative development of decomposition into components *A* and *B*. This can be achieved by choosing $\tilde{\nu}_{BM}^{(A)} < 0$ or $\tilde{\nu}_{BM}^{(M)} > 0$ or $\tilde{\nu}_{BM}^{(AM)} < 0$. We note that an additional stimulus of decomposition of component *B* in the latter case arises directly at the interface of precipitates *A* (i.e., in the region with intermediate concentrations of both components *A* and *M*).

In all the cases, at a certain ratio of parameters, precipitates with a phase intermediate composition (PIC) are formed around precipitates *A*. If component *B* is present in the alloy in the form of a small dopant, $c_B^0 \ll c_A^0$, it can be completely used up for the PIC formation, so the equilibrium state of the alloy becomes three-phase: *M*, *A*, and fine PIC precipitates. The problem of stabilizing the precipitates *A* is reduced to the search for such conditions of the decomposition, under which the PIC phase forms the "locking shell" around precipitates *A*. Our analysis shows that the shell is most pronounced in the case of $\tilde{\nu}_{BM}^{(AM)} < 0$ when the PIC contains all the components in approximately equal proportions. Therefore, we further restrict ourselves to discussing the situation $\tilde{\nu}_{BM} = \tilde{\nu}_{BM}^0 + \tilde{\nu}_{BM}^{(AM)} c_A c_M$; i.e., we do not consider the appearance of intermediate phases due to other energy parameters, except for $\tilde{\nu}_{BM}^{(AM)} < 0$.

In Figs. 8–10, the decomposition kinetics is described by equations (6) and proceeds with the formation of an intermediate phase. Precipitates of component *A* are highlighted in gray, the matrix phase is

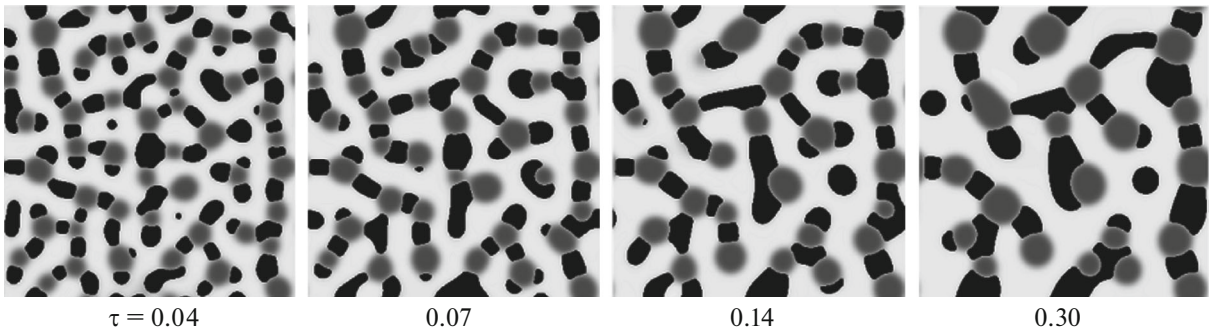

Fig. 8. Kinetics of spinodal decomposition at $D_A^{(M)} = D_B$, $D_A^{(\mathrm{PIC})} = 10^{-3}$; $c_A^0 = 0.30$, $c_B^0 = 0.07$, $\tilde{\nu}_{AM}/kT = -3.5$, $\tilde{\nu}_{BM}^0 = \tilde{\nu} = 0$, $\tilde{\nu}_{BM}^{(AM)}/kT = -100$, $\sigma_{A(B)}(R/L)^2/kT = 4 \times 10^{-4}$, and $\sigma_{AB} = 0$.

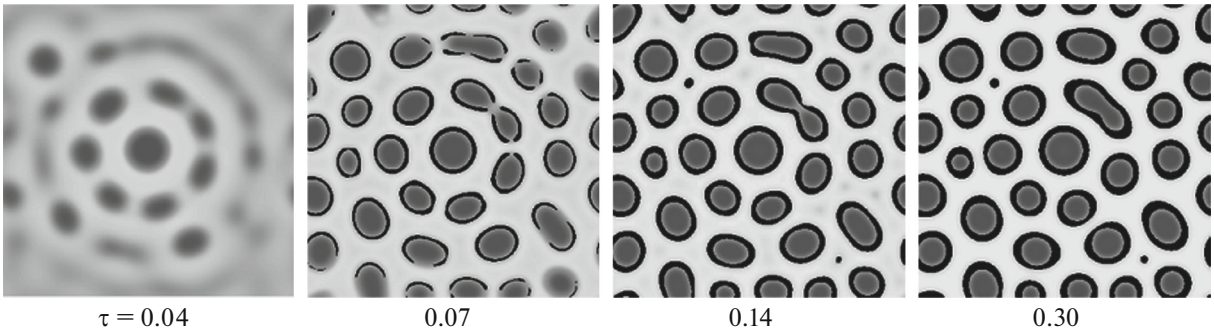

Fig. 9. Kinetics of spinodal decomposition at $D_B^{(M,\mathrm{PIC})} = 10^{-2}$, $D_B^{(A)} = 3 \times 10^{-3}$, and $D_A^{(\mathrm{PIC})}/D_A^{(M)} = 10^{-3}$. The remaining parameters are same as those in Fig. 8.

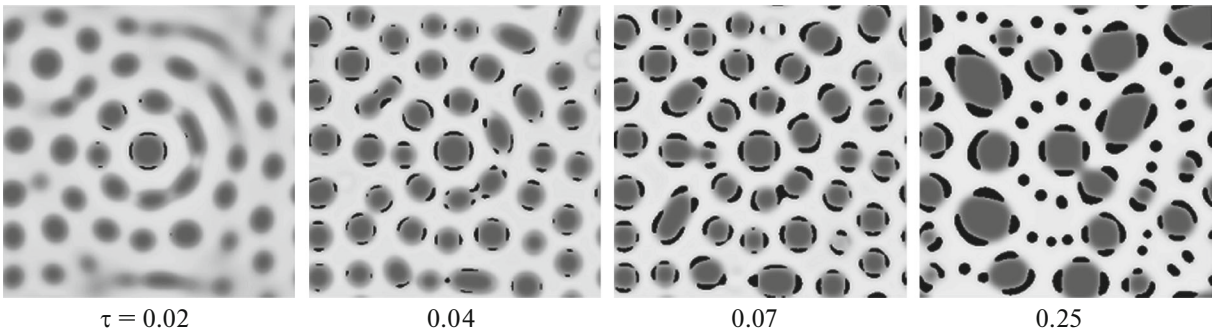

Fig. 10. Kinetics of spinodal decomposition at $c_B^0 = 0.05$, $D_B^{(M,\mathrm{PIC})}/D_A = 10^{-2}$, $D_B^{(A)}/D_A = 1$. The remaining parameters are same as those in Fig. 8.

highlighted in white, and PIC precipitates are highlighted in black. The morphology of the precipitates is largely determined by the ratio of the diffusion coefficients of the components. At $D_A^{(M)} \sim D_B^{(M)}$ and a sufficient concentration of atoms of both types, the microstructure of chains of alternating precipitates A and PIC is formed (Fig. 8). A similar picture was observed earlier in [15] for spinodal decomposition in a three-component alloy.

If the diffusion rate of component B in the matrix is significantly lower than the diffusion rate of component A ($D_B^{(M)} \ll D_A^{(M)}$), a microstructure from the precipitates of component A surrounded by a PIC shell (Fig. 9) is formed. In this case, for the appearance of

the shell, the displacement of component B from the volume of growing precipitates A is necessary. Therefore, at a decrease in the coefficient $D_B^{(A)}$, the shell arises at later decomposition stages when the growth rate of precipitates becomes already sufficient low. The precipitates surrounded by the shell are formed at an intermediate stage of decomposition and coagulate at long exposure times due both to the combination of PIC particles and diffusion of component A through the shell. A decrease in the average concentration c_B^0 leads to a situation where, at the time of the PIC formation, component B near the precipitate is insufficient. In this case, an intermittent shell appears around precipitate A, which is not a reliable stop for the development of decomposition (Fig. 10).

The main difference between the considered situation and the case of the shell formation from a pure component (Section 4) is as follows. Since the PIC contains a significant amount of component A, it generally remains "transparent" for diffusion of this component from the matrix volume to a growing precipitate and does not inhibit the growth of precipitates A. However, a significant decomposition retardation is achieved if the diffusion coefficients of components A or B in the region of the PIC phase are significantly lower than the diffusion coefficient of component A in the matrix; $D_A^{(\mathrm{PIC})} \ll D_A^{(M)}$ or $D_B^{(\mathrm{PIC})} \ll D_A^{(M)}$. In the first case, component A is supplied to the precipitate through the shell and it is difficult while, in the second case, the increase in the precipitate A implies the migration of the shell enriched with slow component B.

Figures 11a and 11b show the change in the maximal size of the precipitate of component A and the dispersion extent at various ratios of the diffusion coefficients in phases. Curve A matches completely frozen diffusion of component B ($D_B = 0$). In this case, the maximal size of the precipitates monotonically increases, and the dispersion extent reaches a maximum at the end of the wave stage of the spinodal decomposition, after which it decreases monotonously. Curves *2* and *3* are plotted at various values of $D_B^{(M,A)}$, but in the absence of a decrease in the diffusion mobility of component A in the PIC region ($D_A^{(\mathrm{PIC})} = D_A^{(M)}$). From a comparison of curves *1*–*3*, it follows that a low coefficient $D_B^{(M)}$ slows down the decomposition of component A, as it helps to stabilize the shell.

Curves *4* and *5* are plotted taking into account the inhibition of diffusion of component A in the PIC ($D_A^{(\mathrm{PIC})} \ll D_A^{(M)}$) and differ only by the value of the diffusion coefficient $D_B^{(A)}$. As can be seen in the figure, a high coefficient $D_B^{(A)}$ more effective stabilizes precipitate A at the initial stages due to the rapid formation of the shell, but then decomposition proceeds slowly due to the shell destruction. The most effective stabilization of dispersed precipitates at the evaporation-condensation stage is achieved for curve *4*, which corresponds to the case of $D_A^{(\mathrm{PIC})} \ll D_A^{(M)}$, $D_B^{(M,A)} \ll D_A^{(M)}$ (Fig. 9).

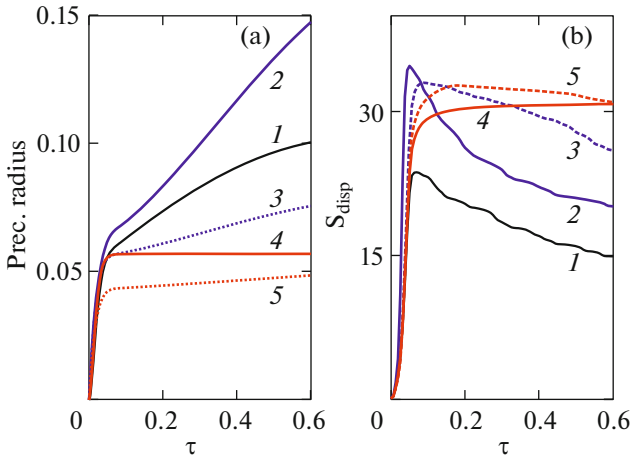

Fig. 11. Evolution (a) of the maximal size of the precipitate and (b) the dispersion extent of the precipitates at (*1*) $D_B = 0$; (*2*) $D_B^{(M,\mathrm{PIC})} = 10^{-1}$, $D_B^{(A)}/D_A^{(M)} = 1$, $D_A^{(\mathrm{PIC})}/D_A^{(M)} = 1$; (*3*) $D_B^{(M,\mathrm{PIC})}/D_A^{(M)} = 10^{-2}$, $D_B^{(A)}/D_A^{(M)} = 1$, $D_A^{(\mathrm{PIC})}/D_A^{(M)} = 1$; (*4*) $D_B^{(M,\mathrm{PIC})}/D_A^{(M)} = 10^{-2}$, $D_B^{(A)}/D_A^{(M)} = 3 \times 10^{-3}$, $D_A^{(\mathrm{PIC})}/D_A^{(M)} = 10^{-3}$; and (*5*) $D_B^{(M,\mathrm{PIC})}/D_A^{(M)} = 10^{-2}$, $D_B^{(A)}/D_A^{(M)} = 1$, $D_A^{(\mathrm{PIC})}/D_A^{(M)} = 10^{-3}$. The remaining parameters are same as those in Fig. 8.

6. DISCUSSION AND CONCLUSIONS

The kinetics of the growth of coherent precipitates from a supersaturated solid solution in a three-component alloy is studied. The effective mechanism of decomposition inhibition is shown to be the formation of a continuous either intermittent "locking" shell in the form of a layer of a new phase around the precipitate particles, in which the solubility or diffusion coefficients of alloy components are decreased. As a result of the appearance of such the shell, the matter supply to the growing precipitate is blocked, and therefore, the dispersed state is stabilized.

The reason for the appearance of the shell can be kinetic (Fig. 1) or thermodynamic factors (Figs. 2–5), or their combined action (Figs. 9 and 10). Therefore, the shell properties are qualitatively different: in particular, equilibrium enrichment of the interphase boundary with an impurity (Figs. 2 and 3) and isolation of either component B in its pure form (Figs. 4, 5, and 7) or the phase with an intermediate composition at the interphase boundary (Figs. 9 and 10) may occur. The shell formation is favored by the low diffusion rate of component B in the matrix after its displacement from the precipitate volume, $D_B^{(M)} \ll D_A^{(M)}$, as well as in

the precipitate volume, $D_B^{(A)} \ll D_A^{(M)}$ (Figs. 1, 5, and 9). At a high diffusion rate of component B, solitary precipitates of this component or a branching structure of alternating precipitates of two types arise (Fig. 8).

The performed analysis shows that the shell formation around the precipitate does not always promote slowing down the decomposition kinetics. For example, the properties of the kinetically determined shell (Fig. 1) usually slightly differ from the bulk properties of the alloy. The shell has a variable width and amplitude of the concentration change and should lead to decomposition inhibition mainly at the early stages.

Note that the decomposition inhibition at the evaporation-condensation stage (Ostwald ripening) as a result of the formation of a kinetically determined shell was observed in the Al–Zr–Sc alloy [14]. This alloy has a specific ratio of the diffusion coefficients of components $D_{\mathrm{Sc}}^M \gg D_{\mathrm{Zn}}^M$, $D_{\mathrm{Sc}}^P \approx 0$, and $D_{\mathrm{Zn}}^P \approx 0$, where $D_{\mathrm{Sc(Zn)}}^M$ and $D_{\mathrm{Sc(Zn)}}^P$ are the diffusion coefficients of Sc and Zr impurities in the aluminum matrix and in the volume of $Al_3Sc_xZr_{1-x}$ precipitates, respectively. At the initial stages of decomposition, the $D_{\mathrm{Sc}}^M \gg D_{\mathrm{Sn}}^M$ condition provides the growth in Al_3Sc precipitates from a supersaturated solid solution in the absence of a noticeable Zr diffusion. However, at the evaporation–condensation stage, the characteristic times of the decomposition kinetics are comparable with the times of Zr diffusion in the matrix. Therefore, a shell forms around the Al_3Sc precipitates enriched with Zr. In this case, the $D_{\mathrm{Sc}}^P \approx 0$ condition prevents the diffusion of Sc atoms through the shell while the $D_{\mathrm{Zn}}^P \approx 0$ condition ensures the impossibility of a uniform distribution of Zr atoms over the selection volume. As a result, the exchange of Sc atoms between precipitates is blocked by zirconium, so that the dispersed state alloy is stabilized.

The shell formed due to the achievement of local equilibrium in the transition layer at the interphase boundary (Figs. 2 and 3) was observed experimentally [17] and in the numerical modeling with CALPHAD parameterization [16] in the Fe–Cu–Ni(Mn) alloy. The shell has a width of the order of the interface boundary and usually has a small amplitude of concentration changes. Monte Carlo simulation [18] showed that such a shell does not inhibit decomposition, but the observed in experiment [17] increase in the dispersion of precipitates in the Fe–Cu–Ni(Mn) alloy is due rather to the accelerated nucleation of copper clusters at impurity centers. At the same time, as part of a combined approach involving Monte Carlo and molecular dynamics modeling, it was shown [25] that the shell formation can lead to inhibition of the particle growth in the Fe–Cu–Ni–Al alloy.

A very effective inhibition of the particle growth precipitated from a metastable supersaturated solid solution occurs when component B has a high stimulus to decompose and precipitates at the interface of precipitate A in its pure form, blocking substance supply to the precipitate (Fig. 4). At the decomposition in the spinodal region of the phase diagram, the formation of such a shell requires an additional condition $D_B \ll D_A$ since, otherwise, the alloy decomposes in the alloy volume by component B, even before the occurrence of precipitates A. In this case, the modeling results shows that, up to very high concentrations c_B^0 around precipitates A, chains of small precipitates of component B rather than a solid shell are formed, which, however, are sufficient for decomposition inhibition (Figs. 5 and 7). Note that the observed effect has some similarities with the pinning phenomenon of grain boundary precipitation preventing the development of the recrystallization process [26].

Another mechanism that inhibits the growth of the precipitates occurs at a low diffusion rate of component A or B through a solid shell, $D_{A(B)}^{\mathrm{PIC}} \ll D_A^{(M)}$ (Fig. 9). This scenario is most likely if the shell is a new phase with an intermediate composition in the general case. The shells resulting from the decomposition with the precipitate of a new phase (Sections 4 and 5) expand until the limit of component B is exhausted and are destroyed at long exposure times due to coagulation of precipitates of their phase. Thus, their formation does not stop the decomposition process. However, it can significantly slow down its kinetics (Figs. 6 and 11).

The conclusions obtained in this study are quite general and remain valid, despite model simplicity and the used approximations (continuum diffusion equations in the mean field approximation, coherent conjugation of precipitates, and the absence of elastic interaction of precipitates). Although most of the results presented here are related to precipitate nucleation by the spinodal mechanism (Figs. 5–11), conclusions about the conditions for stabilization of the dispersed state due to the shell formation around the precipitate should be valid for other (fluctuation and heterogeneous) nucleation scenarios. Note that, in the case of semicoherent precipitates, enrichment of the interphase boundary with an impurity can be realized due to the difference in the energies of the impurity dissolution in the volume and at the interphase boundary [12, 13]. The shells arising in this case have a width equal to the width of the interface boundaries, as the shells have, as considered in Subsection 3.2. However, unlike the latter, they can lead to the appearance of an equilibrium size of precipitates, provided that the energy of impurity segregation at the interface exceeds a certain critical value [12, 13].

FUNDING

This work was carried out as part of the state assignment on the topics "Magnet," no. A18-118020290129-5 and "Structure," no. A18-118020190116-6, and was supported

by the Russian Science Foundation, project no. 18-12-00366.

CONFLICT OF INTEREST

The authors declare no conflicts of interest.

REFERENCES

1. S. Jiang, H. Wang, Y. Wu, X. Liu, H. Chen, M. Yao, B. Gault, D. Ponge, D. Raabe, A. Hirata, M. Chen, Y. Wang, and Z. Lu, Nature (London, U.K.) **544** (7651), 460 (2017).
2. J. Millan, S. Sandlobes, A. Al-Zubi, T. Hickel, P. Choi, J. Neugebauer, D. Ponge, and D. Raabe, Acta Mater. **76**, 94 (2014).
3. R. S. Rana, R. Purohit, and S. Das, Int. J. Sci. Res. Publ. **2**, 1 (2012).
4. F. Sun, J. Y. Zhang, P. Vermaut, D. Choudhuri, T. Alam, S. A. Mantri, P. Svec, T. Gloriant, P. J. Jacques, R. Banerjee, and F. Prima, Mater. Res. Lett. **5**, 547 (2017).
5. O. Gutfleisch, in *Nanoscale Magnetic Materials and Applications*, Ed. by J. P. Liu, E. Fullerton, O. Gutfleisch, and D. J. Sellmyer (Springer, Berlin, 2009).
6. Z. B. Jiao, J. H. Luan, M. K. Miller, Y. W. Chung, and C. T. Liu, Mater. Today **20**, 142 (2017).
7. M. D. Mulholland and D. N. Seidman, Acta Mater. **59**, 1881 (2011).
8. L. Schemmann, S. Zaefferer, D. Raabe, F. Friedel, and D. Mattissen, Acta Mater. **95**, 386 (2015).
9. M. Perez, F. Perrard, V. Massardier, X. Kleber, A. Deschamps, H. de Monestrol, P. Pareige, and G. Covarel, Philos. Mag. **85**, 2197 (2005).
10. A. G. Khachaturyan, *Theory of Phase Transformations and the Structure of Solid Solutions* (Nauka, Moscow, 1974) [in Russian].
11. T. Miyazaki, Mater. Trans. **43**, 1266 (2002).
12. I. K. Razumov, Phys. Solid State **56**, 780 (2014).
13. S. B. Kadambi and S. Patala, Phys. Rev. Mater. **1**, 043604 (2017).
14. E. Clouet, L. Lae, T. Epicier, W. Lefebvre, M. Nastar, and A. Deschamps, Nat. Mater. **5**, 482 (2006).
15. L. Q. Chen, Acta Metall. Mater. **42**, 3503 (1994).
16. T. Koyama and H. Onodera, Mat. Trans. **46**, 1187 (2005).
17. M. K. Miller, B. D. Wirth, and G. R. Odette, Mater. Sci. Eng. A **353**, 133 (2003).
18. Y. Wang, J. Yin, X. Liu, R. Wang, H. Hou, and J. Wang, Prog. Nat. Sci.: Mater. Int. **27**, 460 (2017).
19. S. Ghosh, A. Mukherjeez, T. A. Abinandanan, and S. Bose, Phys. Chem. Chem. Phys. **19**, 15424 (2017).
20. M. S. Bhaskar and T. A. Abinandanan, Comput. Mater. Sci. **146**, 73 (2018).
21. J. Christian, *Theory of Transformations in Metals and Alloys* (Pergamon, Oxford, 1975; Mir, Moscow, 1978).
22. J.-F. Gouyet, M. Plapp, W. Dieterich, and P. Maas, Adv. Phys. **52**, 523 (2003).
23. J. W. Cahn and J. E. Hilliard, J. Chem. Phys. **28**, 258 (1958).
24. B. B. Straumal, *Grain Boundary Phase Transitions* (Nauka, Moscow, 2003) [in Russian].
25. I. N. Kar'kin, L. E. Kar'kina, Yu. N. Gornostyrev, and A. P. Korzhavyi, Phys. Solid State **61**, 601 (2019).
26. T. Chakrabarti and S. Manna, Comput. Mater. Sci. **154**, 84 (2018).

Translated by A. Ivanov